Master in / Máster en

Physics of Condensed Matter and Biological Systems

Física de la materia condensada y los sistemas biológicos

Topological phase and Majorana zero modes in full-shell nanowires

Fase topológica y modos de Majorana en nanohilos encapsulados

Carlos Payá Herrero

Supervisor / Directora: **Elsa Prada Núñez**
Academic Tutor / Tutor académico: Eduardo J.H. Lee
Institution / Lugar de realización: Instituto de Ciencia de Materiales de Madrid,
Consejo Superior de Investigaciones Científicas

Topological phase and Majorana zero modes in full-shell nanowires
Fase topológica y modos de Majorana en hilos híbridos encapsulados

Carlos Payá,[1,2]

Supervisor / Directora: Elsa Prada,[1] ,

Academic Tutor / Tutor Académico: Eduardo J.H. Lee[2]

[1] *Instituto de Ciencia de Materiales de Madrid, Consejo Superior de Investigaciones Científicas (ICMM-CSIC), Madrid, Spain*
[2] *Departamento de Física de la Materia Condensada and Condensed Matter Physics Center (IFIMAC),*
Universidad Autónoma de Madrid, Madrid, Spain
(Dated: September 19, 2022)

Abstract

In this work we study the electronic spectrum of full-shell nanowires –hybrid systems composed of a semiconductor nanowire with strong spin-orbit coupling (SOC) fully encapsulated by a thin, epitaxially-grown superconductor–, when subject to an axial magnetic field. These wires were brought to the spotlight recently as an alternative nanowire configuration for the creation of Majorana zero modes with several advantages with respect to previous designs. We analyze the bandstructure and the local density of states (LDOS) at one end of semi-infinite such wires, which presents a rich phenomenology. On the one hand, and due to the cylindrical geometry of the superconducting shell, the system exhibits the Little-Parks (LP) effect, whereby the superconducting gap is modulated periodically with magnetic flux in units of the superconducting flux quantum Φ_0, forming a series of lobes labelled by the number of the *fluxoid* quanta threading the hybrid wire, $n = 0, \pm1, \pm2....$ On the other hand, and due to the confining potential produced by the normal-superconducting interface, the nanowire core develops subgap Andreev bound states that are the hybrid-wire analogs of the Caroli-de Gennes-Matricon (CdGM) states in vortices of type II-superconductors. These CdGM analogs are in fact shell-induced Van Hove singularities in propagating core subbands. Given a strong enough SOC, the system can undergo a topological phase transition an exhibit Majorana bound states (MBSs) at its ends, which appear as zero bias peaks (ZBPs) in the LDOS. We study the behavior of these ZBPs, as well as other subgap states, with a number of models of increasing complexity, all applied to the experimentally relevant case of InAs/Al hybrid wires. We start with a simple, analytically-solvable model known as the hollow-core approximation, where all the semiconductor charge is assumed to be located at the superconductor/semiconductor interface. The CdGM Van-Hove states disperse with flux within each LP lobe with positive or negative slope depending on their angular momentum. In the hollow-core case, all the Van-Hove singularities in LDOS cross at the center of the LP lobes, where the hybrid wire is threaded by an integer value of Φ_0, forming a so-called degeneracy point. If the wire is in the topological phase, ZBPs appear at the edges of odd-n LP lobes, where the flux is close to half-integer values of Φ_0. Going beyond simplistic toy models, we perform microscopic tight-binding (TB) simulations of the hybrid wires. First we add a finite thickness to the semiconductor core in what we call the tubular model. We observe that the CdGM degeneracy point shifts towards larger values of the magnetic flux within each lobe as we increase the semiconductor thickness, breaking the previous symmetry of subgap states around the lobe center, and extending the left MBS-ZBP to larger values of the flux, while the right one disappears. This ZBP eventually extends all along odd LP lobes in the solid-core limit. Finally, we consider a realistic radial dome profile for the electrostatic potential of ohmic superconducting-semiconducting heterostructures, finding that in this case the system behaves similarly than with the tubular model of a finite semiconductor width. For realistic wires, Majorana-driven ZBPs can be obtained for a range of dome profiles for wires with strong SOC, typically one order of magnitude larger than the nominal values. Interestingly, the behaviour of the CdGM analogs is barely affected by the SOC.

Resumen

En este trabajo estudiamos el espectro electrónico de nanohilos encapsulados – sistemas híbridos compuestos por un nanohilo semiconductor con fuerte acomplo espín-órbita (en inglés, SOC) completamente encapsulado por una capa de poco grosor de un superconductor crecido epitaxialmente – sujetos a un campo magnético axial. Estos hilos han sido el centro de atención de recientes investigaciones como una configuración alternativa para la creación de modos de Majorana con diversas ventajas respecto a los diseños previos. En particular, analizamos la densidad local de estados (LDOS en inglés) en el borde de un hilo semi-infinito como los descritos, presentando una rica fenomenología. Por un lado, debido a la geometría cilíndrica del recubrimiento superconductor, el sistema exhibe el efecto Little-Parks (LP), por el cual el gap superconductor se modula periódicamente con el flujo magnético en unidades del cuanto de flujo superconductor, Φ_0, formando una serie de lóbulos etiquetados por el número de cuantos de fluxoide que atraviesan el hilo, $n = \pm 1, \pm 2, ...$ Por otro lado, debido al potencial de confinamiento producido por la interfase normal-superconductor, el núcleo del nanohilo desarrolla estados ligados de Andreev en el interior del gap que son análogos en hilos híbridos a los estados Caroli-de Gennes-Matricon en vórtices de superconductores tipo II. Estos estados CdGM son de hecho singularidades de Van Hove inducidas por la corteza en las sub-bandas propagantes del núcleo. Dado un SOC lo suficientemente fuerte, el sistema atraviesa una transición topológica y exhibe estados ligados de Majorana (MBS en inglés) en sus extremos, que aparecen como picos de voltaje cero (ZBP en inglés) en la LDOS. Estudiamos el comportamiento de estas ZBP así como de otros estados en el interior del gap, con diversos modelos de creciente complejidad aplicados al caso relevante experimentalmente de hilos híbridos InAs/Al. Comenzamos con un modelo simple y resoluble analíticamente conocido como modelo hollow-core (núcleo hueco), donde se asume que toda la carga del semiconductor está localizada en la interfase superconductor/semiconductor. Las singularidades CdGM Van Hove dispersan con el flujo en cada lóbulo LP con pendiente positiva o negativa dependiendo de su momento angular. En el caso hollow-core, todas las singularidades Van Hove en la LDOS se cruzan en el centro de los lóbulos LP, donde el hilo híbrido es atravesado por un valor entero de Φ_0, formando lo que hemos denominado punto de degeneración. Si el hilo está en la fase topológica, aparecen ZBP en los bordes de los lóbulos LP con n impar, donde el flujo está cerca de un valor semientero de Φ_0. Yendo más allá de los modelos analíticos simplistas, realizamos simulaciones microscópicas *tight-binding* de los hilos híbridos. En primer lugar, añadimos un grosor finito al núcleo semiconductor en lo que llamamos modelo tubular. Observamos que el punto de degeneración de los CdGM se desplaza a valores mayores del flujo magnético en cada lóbulo según aumenta el grosor del semiconductor, rompiendo la simetría previa de los estados en el interior del gap alrededor del centro del lóbulo, y extendiendo el MBS-ZBP izquierdo a valores mayores del flujo, mientras que el derecho desaparece. Este ZBP finalmente se extiende a lo largo de cada lóbulo LP en el límite de núcleo sólido (solid-core). Finalmente, consideramos un potencial tipo cúpula radial realista para el potencial electrostático de estructuras óhmicas superconductor/semiconductor, encontrando que en este caso el sistema se comporta de forma similar al modelo tubular de un cierto grosor finito. Para hilos realistas, se pueden obtener ZBP inducidos por MBS para un cierto rango de perfiles de potencial y fuerte SOC, cono valores típicamente un orden de magnitud superiores al nominal. Es llamativo que el comportamiento de los análogos CdGM apenas se ve afectado por el SOC.

I. INTRODUCTION

Topological superconductors have been studied in condensed matter physics since the beginning of the century due to the fascinating properties of topological materials combined with the superconducting phase [1–6]. Back in 2001, Kitaev [7] proposed his famous toy-model for a one-dimensional topological superconductor. In the topological phase, the system develops edge states at the wire ends with several interesting properties. These in-gap Bogoliuvov zero energy excitations, that are topologically protected by the electron-hole symmetry of the Bogoliubov-de Gennes (BdG) Hamiltonian, and whose fermionic creation operators are equal to their adjoint, are known as Majorana bound states (MBSs). However, they do not follow fermionic statistics, but a non-abelian one, making them good candidates for a topological qubit.

As the Kitaev model needs a spinless fermionic liquid and superconductivity, a p-wave superconductor is, *a priori*, required. However, in 2008 Fu and Kane [8] proposed a way to obtain this condition by proximizing an s-wave superconductor to a topological insulator. In 2010, Lutchyn *et al.* and Oreg *et al.* [9, 10] designed a simpler theoretical model in which a semiconductor nanowire with strong spin-orbit coupling (SOC), in contact to a conventional superconductor and subject to an external magnetic field B, reproduces the Kitaev conditions. Through the Zeeman effect, given a certain B, the system undergoes the topological phase transition, marked by a band inversion, producing MBSs at its ends. Since this hybrid system, also known as the Majorana nanowire, is amenable to be realized in a laboratory, it has been extensively studied both theoretically and experimentally (see Ref. 1 or 2 for an extensive review on the subject.). However, after several detections of zero bias peaks (ZBPs) in tunneling spectroscopy experiments in principle compatible with MBSs, it has been realized in the community that the reality of this nanowires is far more complex than initially assumed with minimal models [1, 11–13]. Unfortunately, there are several trivial mechanisms in realistic nanowires that can simulate MBS signals, so new geometries and experimental devices, built with higher quality materials and that go beyond in local spectroscopy, have been recently studied.

One of the inconveniences of the Oreg-Luthcyn proposal is that high intensity magnetic fields are required to achieve the topological transition, closing the superconducting gap before the transition can occur [14]. Recently, a new nanowire design has been proposed in the literature that could overcome this problem, as well as to present several advantages. Instead of using a semiconductor nanowire with only some of its facets covered by the superconductor, which is the the traditional Majorana nanowire, it has been proposed and realized the use of so-called full-shell nanowires [15]. In a full-shell nanowire, a thin superconducting shell, typically grown epitaxially over the semiconductor, completely covers the semiconducting core all around. In these wires, the topological phase transition is not driven by the Zeeman effect, like in the Oreg-Lutchyn proposal, but by the orbital effect induced by the magnetic flux Φ threading the wire in the presence of an axial field B [15]. It needs lower magnetic fields to drive the nanowire into the topological state, and the MBSs are predicted to appear at specific values of Φ, making its unequivocal detection somewhat easier.

This new system, schematically depicted in Fig. 1(a), has moreover demonstrated to have a very rich phenomenology [16–20], even outside the topological phase, due mainly to the doubly-connected geometry of the superconductor, i.e., to the fact that the superconductor has the shape similar to a cylinder. Firstly, the Little-Parks (LP) effect arises, that is, the modulation of the superconductor critical temperature (or gap Δ) as a function of the axial magnetic flux Φ. Due to the superconductor cylindrical shape, the phase of the superconducting order parameter acquires an integer winding, known as the winding number, $n \in \mathbb{Z}$. This is also known as the *fluxoid* number, since it coincides with the number of fluxoid quanta, in units of $\Phi_0 = h/2e$, that threads the superconductor in the presence of a magnetic field. Note that in this system, the fluxoid and not the flux is quantized. In the LP effect, Δ is maximum at $\Phi = n\Phi_0$ and minimum, or even zero in the LP destructive regime, at $\Phi = \frac{n}{2}\Phi_0$ forming a series of so-called LP lobes with Φ_0 periodicity, as illustrated in Fig. 1(b). This effect, mainly controlled by the geometry of the system and the superconductor coherence length, ξ, is well-known both experimentally and theoretically [21–25] since the 60s. However, the theory used in this research was developed a decade ago [26, 27].

Secondly, the normal and Andreev reflections at the superconductor/semiconductor interface give raise to states analog to Caroli-de Gennes-Matricon states (CdGM) in Abrikosov vortex lines of type-II superconductors [24, 28–30], which have been studied in a recent publication [31]. CdGM analog states in nanowires were found to emerge from shell-induced Van Hove singularities in the quasi-one dimensional propagating subbands that propagate along the semiconducting core [31]. However, the key to allow for a topological transition in nanowires, as was also the case in the original toy-model proposal by Oreg *et al.* and Lutchyn *et al.* [10, 32], is the SOC. In the study of subgap states in full-shell nanowires done in Ref. 31, this effect was neglected as it is not relevant away form the topological phase. In this master thesis, we describe how the SOC impacts the system both in the trivial and topological regimes, starting from the simplest full-shell nanowire model and adding features that get it closer to the experiment.

We use a cylindrical model of the hybrid nanowire that allows us to characterize the subbands of the system in terms of a generalized angular momentum number m_J. Then, for a semi-infinite full-shell nanowire, we compute the local density of states (LDOS) at its end. For the
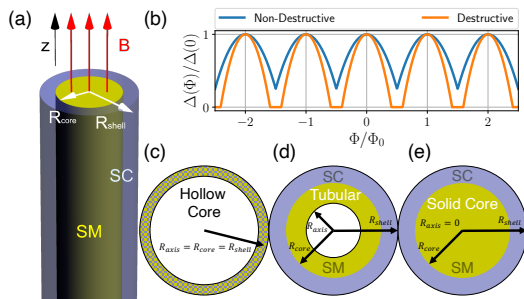
Figure 1. **Full-Shell nanowire models and Little-Parks effect.** **(a)** Schematic of the cylindrical model used for a semi-infinite full-shell nanowire. The semiconducting core in yellow, with radius R_{core}, is covered all around by a thin superconducting shell in blue, of width $R_{shell} - R_{core}$. The hybrid system is penetrated by an axial magnetic field B in the z direction. **(b)** Sketch of the Little-Parks (LP) effect. The doubly-connected geometry of the superconducting shell induces a modulation of the superconducting gap, Δ, as a function of the magnetic flux Φ, with period Φ_0 (the superconducting flux quantum). This modulation gives rise to so-called LP lobes, where the gap is maximum around integer values of the normalized flux, and minimum at half-integer ones. Depending on the effective LP radius $R_{LP} = (R_{core} + R_{shell})/2$, and the superconducting coherence length, ξ, the gap may be zero at the lobe edges (destructive regime) or finite (non-destructive regime). Due to the proximity effect, superconducting correlations are induced in the semiconducting core. **(c,d,e)** Axial cut of the three models studied. Introducing a fictitious inner radius R_{axis} for the semiconductor, the hollow-core model (c) corresponds to the case where all the charge density is assumed to be loceled at the superconducting-semiconducting interface, so that $R_{shell} = R_{core} = R_{axis}$. In the tubular model (d), the semiconductor has a finite thickness, $R_{core} - R_{axis}$. Finally, the solid-core model (e) has no empty region inside ($R_{axis} = 0$) and thus it is the closest to reality. It is the one represented in (a).

parameters of the system, we use the ones of an InAs core, and an Al shell, as these are the materials used in recent experiments [15, 20, 33].

This report is organized as follows. First, in Sec. II, we discuss how the LP effect affects superconductivity in our system; then, in Sec. III, we use a hollow-core model, effectively one dimensional, that can be solved analytically, to carefully analyze the effect of the SOC in these hybrid nanowires. In this model, we take the fictitious inner radius of the semiconductor cylinder, R_{axis}, to be equal to the outer one, R_{core}, and to the superconductor external radius R_{shell}, as shown in Fig. 1(c). We compare the band structure of the system with and without SOC and obtain a phase diagram for the topological phase as a function of the SOC parameter and the chemical potential of the system, commenting on the role of the superconductor penetration length and the Zeeman effect. In Sec. IV we introduce a finite thickness for the semiconductor, making $R_{axis} < R_{core}$ as illustrated in Fig. 1(d). We call this the tubular model. To take into account the superconducting proximity effect in a numer-

ically accessible manner, we integrate-out the superconductor and include its effect on the semiconductor core as a self-energy at the core's outer radius. Finally, we reach the realistic solid-core situation, where $R_{axis} = 0$ [Fig. 1(e)], in Sec. V, where apart from considering the case of a constant chemical potential, we also consider a more realistic scenario where the semiconductor electrostatic potential has a radial dome profile, characteristic of a superconductor/semiconductor ohmic contact. Finally, we discuss our results and give our conclusive remarks in Sec. VI.

II. THE LITTLE-PARKS EFFECT

We describe superconductivity with a pairing potential $\Delta(\vec{r})$. Through this report, we use $\Delta = \Delta(\Phi)$. Since this order parameter is single-valued, its phase must change by $n \in \mathbb{Z}$ at each 2π loop around the shell ring, that is, in cylindrical coordinates $\vec{r} = (r, \varphi, z)$, with the nanowire axis at z,

$$\Delta(\vec{r}) = \Delta e^{in\varphi}. \tag{1}$$

This integer number is $n = \Phi'/\Phi_0$, the fluxoid. Φ' is known to be quantized in units of Φ_0 for multiply-connected superconductors since the very first studies on superconductivity. F. London [34] defined the fluxoid as the magnetic flux Φ perturbed by the circulation of persisting supercurrents induced by Φ. For very thin superconductors, our case, the Meissner effect is negligible [35, 36], so the persistent supercurrents do not vanish anywhere in the superconductor and thus the flux is not quantized. The screening supercurrents term oscillates with the flux as the fluxoid increases in units of Φ_0, inducing a modulation of Δ with period Φ_0. This is known as the LP effect [21, 22, 24, 25]. Schwiete and Oreg [27] demonstrated that this effect can be modeled analogously to paramagnetic impurities, leading to a compact set of transcendental equations that very precisely compute the LP lobes, showing two distinct regimes. In the destructive regime, orange in Fig. 1(b), for certain fluxes around half integer values of Φ/Φ_0, where the flux performs abrupt first order transitions, the pairing goes to zero. In the non-destructive regime, blue in Fig. 1(b), at $\Phi/\Phi_0 = n/2$, Δ reaches its minimum. This second regime is valid when $R_{shell}/\xi > 0.6$ and $R_{shell} \gtrsim R_{core}$. Typical experimental values [15] are $R_{core} \sim 70$nm, $R_{shell} \sim 80$nm, $\xi \sim 100$nm, so our calculations are performed in the non-destructive regime. Fortunately, this scenario allows for another much simpler parametrization of the gap [23, 31]

$$\frac{\Delta(\Phi)}{\Delta(0)} = 1 - \gamma \left(\frac{\Phi}{\Phi_0} - n \right)^2, \tag{2}$$

with

$$\gamma = 4 \left(1 - \frac{\Delta\left(\frac{1}{2}\Phi_0\right)}{\Delta(0)} \right). \tag{3}$$

III. HOLLOW-CORE NANOWIRE

A. Model

Following Ref. 15, we write a Hamiltonian that takes into account the effect of the magnetic flux on the shell (modulated by the LP effect) and on the core subbands. We use a cylindrical approximation for the hybrid wire and thus cylindrical coordinates as described in the previous section. We start with the simplest possible model for this system, called the hollow-core model, where we consider that all electrons are located at the superconductor/semiconductor interface, so there is no radial coordinate, $r = R_{core}$ (see Fig. 1(c)). Ignoring the Zeeman effect, since it has a small effect for the small magnetic fields needed, the Hamiltonian of the core takes a very simple expression

$$H_0 = \frac{(\vec{p} + eA_\varphi \hat{\varphi})^2}{2m^*} - \mu + \alpha \hat{r} \left[\vec{\sigma} \times (\vec{p} + eA_\varphi \hat{\varphi}) \right], \quad (4)$$

where $A_\varphi = \Phi(R_{core})/2\pi R_{core}$ is the angular component of the vector potential, μ is the semiconductor chemical potential, m^* the electron effective mass, and the last term is the semiconductor Rashba SOC, controlled by the parameter α, with σ the spin Pauli matrices and $e > 0$ the unit charge. We use $\hbar = 1$ and simplify notation saying $\Phi = \Phi(R_{core})$.

1. Bogoliuvov-de Gennes Hamiltonian

We are now able to write the Bogoliuvov-de Gennes (BdG) Hamiltonian of the full system in the Nambu basis $\Psi = (\Psi_\uparrow, \Psi_\downarrow, \Psi_\downarrow^\dagger, -\Psi_\uparrow^\dagger)$,

$$H_{BdG} = \begin{pmatrix} H_0(\vec{A}) & \Delta(\vec{r}) \\ \Delta^*(\vec{r}) & -\sigma_y H_0(\vec{A})^* \sigma_y \end{pmatrix}, \quad (5)$$

where we introduce the proximity effect with an effective pairing through (2) with $\Delta(0) = \Delta_0$. The angular, spin and winding symmetries allow us to define a generalized angular momentum

$$J_z = -i\partial_\varphi + \frac{1}{2}\sigma_z + \frac{1}{2}n\tau_z, \quad (6)$$

where τ are the electron-hole space Pauli matrices, that fulfills $[J_z, H_{BdG}] = 0$, so the eigenstates can be decomposed in generalized angular momentum modes, that is,

$$\Psi_{m_J}(r, \varphi, z) \propto e^{i\left(m_J - \frac{1}{2}\sigma_z - \frac{1}{2}n\tau_z\right)\varphi} \Psi_{m_J}(r, z), \quad (7)$$

with a good quantum number m_J. As the wave function must be single valued, we have

$$m_J \in \begin{cases} \mathbb{Z} & n \text{ odd} \\ \mathbb{Z} + \frac{1}{2} & n \text{ even} \end{cases}, \quad (8)$$

so n odd regions have an odd number of m_J states and n even ones an even number of m_J states, marking clear phase transitions at $\frac{\Phi}{\Phi_0} = \frac{n}{2}$.

We can eliminate the angular dependence of the Hamiltonian using the rotation in (7),

$$\tilde{H}_{BdG} = \left[\frac{\left(m_J - \frac{1}{2}\sigma_z - \frac{1}{2}n\tau_z + eA_\varphi R_{core}\tau_z\right)^2}{2m^* R_{core}^2} + \frac{k_z^2}{2m^*} \right.$$
$$- \mu - \frac{\alpha}{R_{core}} \left(m_J - \frac{1}{2}\sigma_z - \frac{1}{2}n\tau_z + eA_\varphi R_{core}\tau_z \right) \sigma_z$$
$$\left. + \alpha k_z \sigma_y \right] \tau_z$$
$$+ \Delta \tau_x, \quad (9)$$

where we have also used that our system is semi-infinite to apply translation symmetry and change the axial momentum operator p_z for a good quantum number k_z. We write the Hamiltonian in this way to be able to compare it with the ones with radial dependence in the following sections, but it can be simplified to a more manageable expression [15]

$$\tilde{H}_{m_J} = \left[\frac{k_z^2}{2m^*} - \mu_{m_J} \right] \tau_z + V_Z \sigma_z + A_{m_J}$$
$$+ C_{m_J} \sigma_z \tau_z + \alpha k_z \sigma_y \tau_z + \Delta \tau_x, \quad (10)$$

where

$$\mu_{m_J} = \mu - \frac{1}{8m^* R_{core}^2} \left(4m_J^2 + 1 + \phi^2 \right) - \frac{\alpha}{2R_{core}} \quad (11)$$

is the effective chemical potential,

$$V_Z = \phi \left(\frac{1}{4m^* R_{core}^2} + \frac{\alpha}{2R_{core}} \right) \quad (12)$$

the effective Zeeman field and

$$A_{m_J} = -\phi \frac{m_J}{2m^* R_2^2}, \quad (13)$$

$$C_{m_J} = -m_J \left(\frac{1}{2m^* R_{core}^2} + \frac{\alpha}{R_{core}} \right), \quad (14)$$

represent the coupling of J_z with the magnetic field. We use $\phi = n - \frac{\Phi}{\Phi_0}$. Notice that there are only two kinds of regions that periodically alternate depending on the parity of the fluxoid, distinguished by having an even or odd number of m_J, each of them associated to a LP lobe. We also observe that ϕ only enters (10) as ϕ^2, so each lobe has a symmetry axis at $\Phi = n\Phi_0$.

B. Van Hove singularities and phase diagram

We can now diagonalize the Hamiltonian and study the behavior of its subbands. For the sake of simplicity, in these first calculations we switch off the LP gap modulation with flux by setting $\gamma = 0$. As shown in Fig.
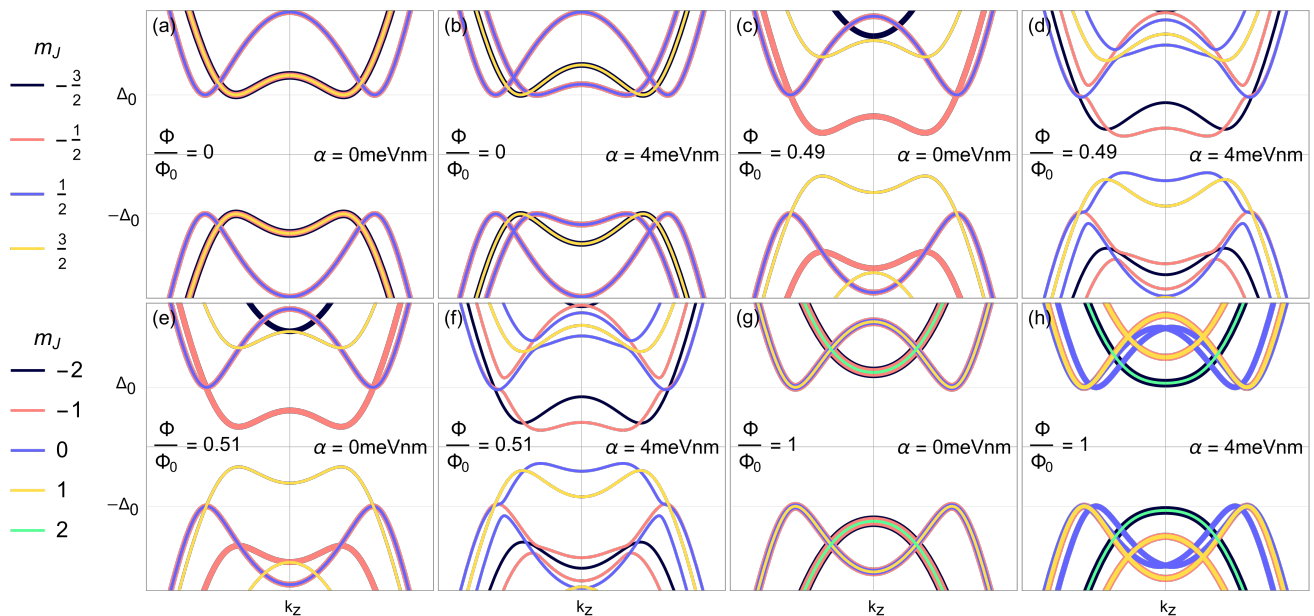
Figure 2. **Effect of SOC on the Nambu bands of a hollow-core nanowire.** BdG dispersion relation on an infinite hollow-core nanowire vs longitudinal momentum k_z (in arbitrary units) for different values of Φ/Φ_0. The energy E is measured with respect to the chemical potential of the superconductor at the middle of its gap. The colors assigned to the different parallel subbands represent their generalized angular momentum quantum number m_J. **(a,b)** In the absence of magnetic field, at the center of the $n = 0$ LP lobe, all subband edges are situated at Δ_0. However, for $\alpha = 0$ the subbands are 4 times degenerate ($\pm m_J$ and spin), while for $\alpha \neq 0$ they are doubly degenerate in $\pm m_J$. **(c,d)** As we increase the flux towards the edge of the $n = 0$ LP lobe, $\Phi/\Phi_0 = 0.49$, the subband minima lie below the parent superconductor gap, leading to Van Hove singularities that we identify as CdGM analog states in the LDOS. A finite flux breaks $\pm m_J$ degeneracy, but positive and negative m_J modes are still degenerate in spin for $\alpha = 0$. Introducing SOC, no subband is degenerate. **(e,f)** Changing to an odd winding number, $n = 1$ in this case, there are now an odd number of subbands. Except for this, the qualitative behavior is the same as before. **(g,h)** At the center of the $n = 1$ LP lobe, where $\Phi/\Phi_0 = 1$, we recover a situation similar to that in (a), where all the subband minima are at energy Δ_0. For these calculations, we have used $m^* = 0.023$, $R_{shell} = R_{core} = 70$nm, $\Delta_0 = 0.23$meV, $\mu = 0.5$meV and neglected the LP gap modulation, $\gamma = 0$.

2, the main feature of these subbands are the avoided crossings. They are induced by Andreev reflections at the shell/core interface and result in Van Hove peaks in the LDOS that disperse with the magnetic flux. We notice that, while the introduction of SOC breaks band degeneracy, the peaks barely shift in energy, or do not even move for integer fluxes. In consequence, the Van Hove singularities are degenerate at the center of each lobe for this thin-shell hollow-core model. As expected, all subbands are symmetric with respect to the $k_z = 0$ axis, and thus show a maximum or minimum in energy at that value of the momentum. It is also relevant to notice that the electron (hole) reflection of a hole (electron) band is not associated with the same m_J but with the opposite one. Hence, an eventual crossing between that pair of subbands cannot produce any kind of bound state or feature in the LDOS since they are not allowed to interact by the symmetries of the Hamiltonian. The only exception to this is $m_J = 0$, a gap closing of this mode at $k_z = 0$ satisfies

$$\Psi_{E,m_J}(k_z) = \Psi_{-E,-m_J}(-k_z), \qquad (15)$$

allowing for the topological transition and the emergence of a MBS.

The Van Hove peaks give raise to what we call CdGM analog states, that we analyze in Fig. 3, where we have plotted the band minima in the first lobe for two values of the SOC parameter. The $m_J = 0$ mode has a richer behavior with α than finite m_J modes. For high enough values of this parameter, CdGM analog states stabilize around a structure similar to that of panel (d), while for zero angular momentum they behave like in panel (c), but no stable structure is reached as the $k_z = 0$ crossing (in red) displaces with the magnetic flux. This crossing is the gap closing that marks the topological transition of the system. As the Hamiltonian is analytically solvable, we can calculate its position for any set of parameters, allowing us to compute a topological phase diagram.

In Fig. 4, we show the phase diagram of the system we have studied in this section. This plots, however, contain more information, since the color represents the length of the topological region inside the odd lobe by means of the lowest possible value of $|\phi|$ for which the system is topological, $|\phi_m|$. Notice that, as we neglect the Zeeman effect, both sides of the lobe are symmetric and thus
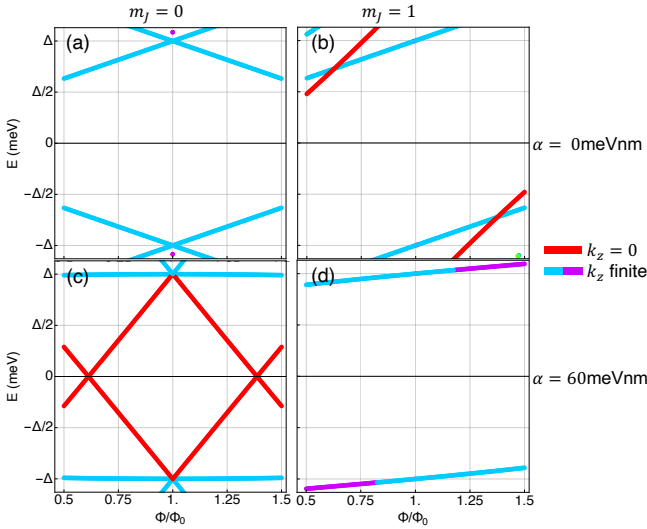
Figure 3. **Energy of the Van Hove singularities in the first LP lobe of a hollow-core nanowire.** Analytically calculated subband minima for $m_J = 0$ (a,c) and $m_J = 1$ (b,d) vs normalized flux in the absence (a,b) and presence (c,d) of SOC. Colors represent the k_z value associated to that band minimum. The system is the same as in Fig. 2. **(a,c)** The $m_J = 0$ mode is the most affected by the introduction of SOC due to the rapid variation with flux of the subband minimum at $k_z = 0$, see red curve in (c). The zero energy crossings at $k_z = 0$ are the gap closings associated to the topological phase transition of the hybrid nanowire. **(b,d)** The subband minima for $m_J = 1$ only weakly depend on flux, specially for the strong α values that allow for a topological phase transition in the first lobe, see (d). Only for very small α a more dispersing $k_z = 0$ Van Hove singularity appears that never crosses zero energy, as seen in (b). We have again neglected the LP effect, considering $\Delta(\Phi) = \Delta_0$. Parameters are as in Fig. 2.
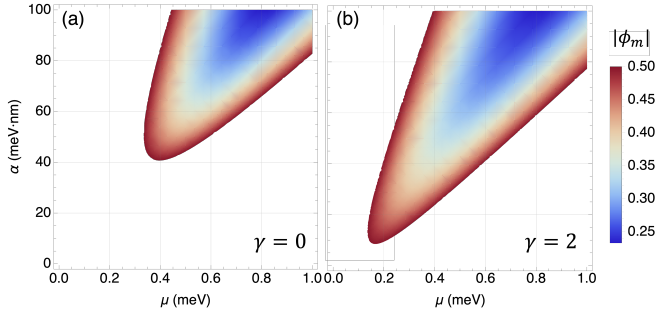

Figure 4. **Phase diagram of a hollow-core nanowire,** as a function of the semiconductor chemical potential μ and the Rashba SOC α. The color scale represents the value of $\phi = n - \Phi/\Phi_0$ in an odd LP lobe at which the topological phase transition takes place, ϕ_m. As the Zeeman effect is neglected, there is no difference between positive and negative ϕ. The trivial region is not colored. In panel (a) we consider $\Delta(\Phi) = \Delta_0$, i.e., $\gamma = 0$, while in panel (b) we consider the LP gap modulation in the non-destructive regime, $\gamma = 2$. Qualitatively, the phase diagram does not change, but larger γ allows to obtain a topological region for significantly lower values of μ and α. Parameters are as in Fig. 2.

twin topological regions appear at both sides of the lobe. For a ZBP associated to a MBS to reach the center of the lobe, that is, having $\phi_m = 0$, we need extremely high values of α and μ. The introduction of the non-destructive LP effect, in panel (b), does not change the phase diagram qualitatively, but allows for topology with smaller values of the Rashba parameter and chemical potential, even if it is just at the very edge of the lobe. We can pictorially understand what is going on with Fig. 3(c), as the LP effect curves de CdGM states and moves the $m_J = 0, k_z = 0$ crossings closer to the center of the lobe, enlarging the topological region at the edges.

C. Local density of states

Now that we have understood the behavior of the CdGM-Van Hove states with SOC from the band structure, we calculate the LDOS at the edge of the nanowire. It is given by

$$\rho(\omega) = -\frac{1}{\pi} \sum_{m_J} \text{Im} G_{m_J}(\omega), \quad (16)$$

where G_{m_J} is the Greens function of the system at the first site of the semi-infinite chain of rings that compose the cylinder and ω the energy explored. We compute this Greens function numerically discretizing our Hamiltonian into a tight-binding (TB) model with just one radial site and converging the discretization parameter a_0 for the angular sites using standard methods [37]. In Fig. 5, we show six examples of LDOS for different values of the SOC parameter as a function of the axial magnetic flux. We have chosen the parameters, which are the same for all figures in this section, so only 5 m_J modes contribute significantly to the LDOS in the first lobe with $\alpha = 0$. This case is shown in panel (a), where all finite m_J CdGM analog states, the intense lines in the plots, are 4 times degenerated, as observed in the band structure. When SOC is switched on (panels (b) to (f)), more and more m_J modes contribute to the total LDOS. Again as predicted from the analytical calculations, the CdGM-Van Hove state associated to $m_J = 0, k_z = 0$ behaves qualitatively differently than the others. It is more intense than the other signals (panel (b)) until topology is allowed, and its curvature is significantly reduced, becoming basically a triangle when the MBS emerges. This is reflected in the LDOS by a strong ZBP. For the α values that allow topology, this state is the slightest of all visible CdGM-Van Hove states. Their behavior reproduces what we obtained from band minima, as illustrated in panel (d), where we have plotted the analytical calculation of Fig. 3(c) adding LP, over the LDOS of the first lobe. There exist some small deviations from the analitical predictions since CdGM analogs are bound states that *hang from* the gap edges and hence can be located at a slightly different energy. All in-gap states, whatever their m_J or k_z, are degenerate for integer fluxes at
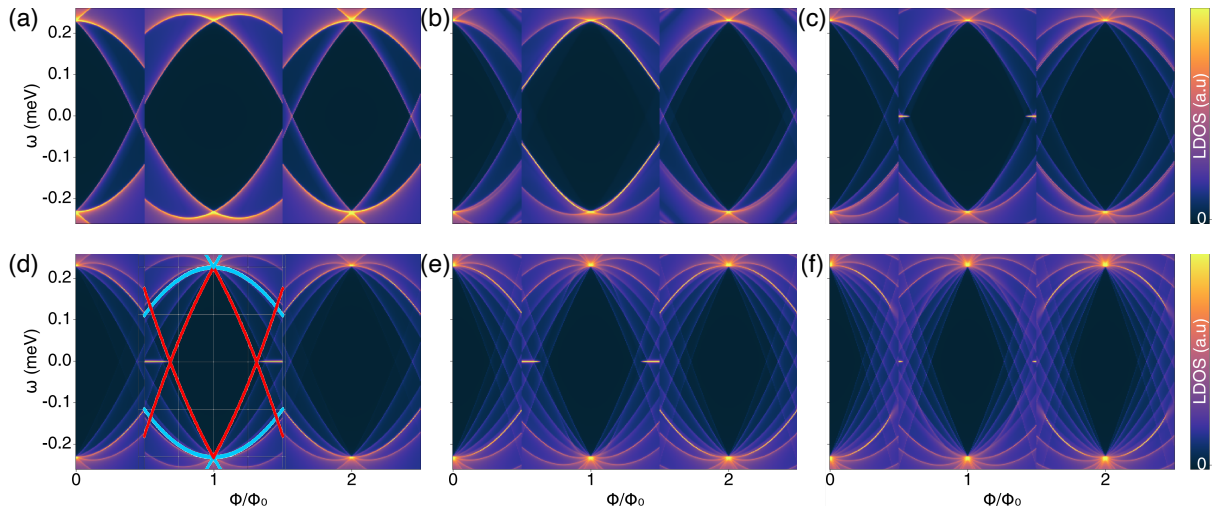
Figure 5. **LDOS at the end of a semi-infinite hollow-core nanowire for different SOC values.** LDOS (in arbitrary units) versus energy ω and applied normalized flux, Φ/Φ_0, displaying half of the zeroth lobe, first and second lobes. The subgap features are CdGM analogs whose bright signals correspond to Van Hove singularities of the different parallel subbands, each of them associated to a m_J and a k_z. The number of CdGM-Van Hove states depends on the semiconductor chemical potential, μ. The induced pairing is LP modulated, $\Delta(\Phi)$. In the hollow-core approximation, all even lobes and all odd lobes are identical, respectively. **(a)** $\alpha = 0$: Without SOC, even and odd lobes look qualitatively similar. The different CdGM-Van Hove states disperse with flux with a slope that is proportional to m_J, and they cross at the degeneracy points at the center of the lobes. They are curved to lower energies close to the lobe edges due to the LP gap modulation. The abrupt transition from even to odd lobes is very clear in this non-destructive LP regime. We have chosen the parameters so that only 5 m_J modes contribute significantly to the LDOS without SOC in the first lobe. They are the same as in previous figures with $\gamma = 2$. **(b)** Same as before but with $\alpha = 10$meVnm: The CdGM analog state associated to $m_J = 0, k_z = 0$ in the $n = 1$ lobe is more intense and has a slightly different shape than the others, with less curvature far from the center of the lobe. We observe that some CdGM-Van Hove states cross at zero energy at the lobe edges, but they are not associated to $m_J = 0, k_z = 0$. As we increase α, more m_J modes contribute to the LDOS because the effective doping of the hybrid nanowire increases. **(c)** $\alpha = 40$meVnm: The bright CdGM-Van Hove state associated to $m_J = 0, k_z = 0$ that we saw in the previous panel has lost most of its intensity, and it has crossings inside the first lobe that cause a topological phase transition. A ZBP is clearly visible at the edges of the first lobe, associated with a MBS appearing at the end of the semi-infinite nanowire. The topological gap is only a true gap for the $m_J = 0$ mode, as other m_J CdGM analog states partially fill that gap. **(d)** $\alpha = 60$meVnm: The situation is pretty similar to the previous panel, but the topological region in flux is larger. Thus, each Majorana ZBP has a larger spread from the LP lobe edge towards the center of the lobe, although it is still pretty localized at the edges. We have overplotted the analytical solution of the band minima in the first lobe. The lines associated to $k_z = 0$ (red) match perfectly, but those with finite k_z (blue) slightly deviate. **(e)** $\alpha = 90$meVnm: The topological region in the odd lobes is shorter than before, because we have exceeded the α value that gives its maximum length in flux. The topological gap is completely filled by $m_J \neq 0$ CdGM analog states. **(f)** $\alpha = 120$meVnm: The topological region has practically disappeared. The behavior of $m_J = 0$ subband is similar to that of panel (c), but now there are more m_J modes (13 of them) that fill partially the true gap (in black). Concerning the even lobes plotted in these simulations, they have a very similar behavior than the odd one, but without any special $m_J = 0$ mode that gives raise to a MBS. These numerical simulations have been performed discretizing the system in steps of $a_0 = 5$nm.

$\omega = \Delta$. This feature, that we call degeneracy point, is key for our discussions in the following sections.

The calculations shown in Fig. 4 for the topological phase and the length of the MBSs are matched perfectly, as shown for example in panel (d). While the topological gap is a true gap for the $m_J = 0$ LDOS, it is partially or even totally filled by other m_J modes in the total LDOS. For the perfectly symmetric system, where different m_J modes cannot couple, this does not affect at all the MBSs. However, if the cylindrical symmetry is broken and m_J is not a good quantum number anymore, the topological region could be seriously affected.

1. A short trip under the carpet

Using the analytical model, we noticed that the equation that gives the parameters of the topological transition has 4 solutions in flux, not only the 2 visible at the first lobe (see for example in Fig. 3(c)). The other two solutions could be complex, but there is nothing that prevents them from being real. Actually, they are real but they simply lie *outside* of the visible region of the odd lobes. If it was possible to vary the flux to larger/smaller values than those of a particular odd lobe, while keeping the fluxoid number fixed, creating a metastable state,
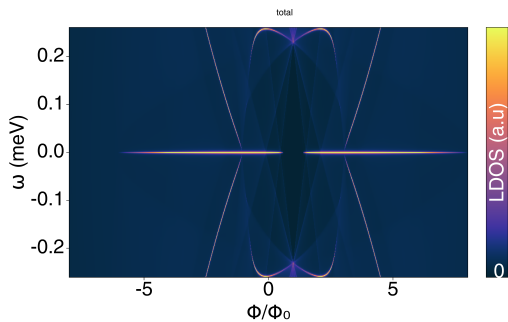
Figure 6. **LDOS at the end of a semi-infinite hollow-core nanowire in the topological regime with forced fluxoid $n = 1$ for all fluxes.** Vertical, dotted lines correspond to the analytical prediction for the flux at which we should observe topological phase transitions. We have used the same parameters as in the previous figures with $\alpha = 60$meVnm, $\gamma = 0$. Forcing the fluxoid to $n = 1$ for all fluxes we can observe the two ends of each topological region, each of them characterized by a $m_J = 0, k_z = 0$ gap closing and reopening. In the first lobe only one of the ends is visible for each topological region, as the fluxoid number changes abruptly with Φ at the edges of the LP lobes.

then we could observe the topological phase transitions associated to the other two solutions. This is what we show in Fig. 6 for a $n = 1$ fluxoid. Those metastable topological transitions are situated precisely where our analytical model predicts them to be. Of course, this is in general not an experimentally achievable situation because it is energetically favourable to change the fluxoid number at the edges of the LP lobes, i.e., at half integer values of the flux quantum. However, it is very interesting to understand that the abrupt appearance of Majorana zero bias peaks at the edges of odd lobes does not come from a topological phase transition, but it is a consequence of first order magnetic Landau transitions.

IV. TUBULAR-CORE NANOWIRE

A. Model

Now that we have observed how SOC affects the simplest hollow-core model, we undo some approximations to get it closer to reality. Instead of an extremely thin shell with just one TB radial site and perfect proximity effect, we consider a tubular wire where the semiconductor has some thickness, as in Fig. 1(d). Therefore, we cannot neglect the radial kinetic term of the Hamiltonian as we did in the previous section. We also introduce the proximity effect by integrating-out the superconducting shell into a self-energy term. There are several possible ways to do this [38, 39], but we choose the one used in Ref. 31 as it is more precise and allows us to define a transparency term $\tau \in [0, 1]$ for the superconductor/semiconductor interface with direct physi-

cal meaning: 1 is transparent junction, 0 means opaque junction. This self-energy also lets us consider a different and finer discretization parameter for the shell, $a_s \ll a_0$, as the Fermi wavelength of Al is much smaller than that of InAs. Defining $t_I = -1/2m_s a_s \sqrt{a_s(a_s + a_0)/2}$, with m_s the effective mass of the superconductor, we have

$$\Sigma_{shell}(\omega) = \tau t_I^2 G_{shell}(\omega, \Delta), \qquad (17)$$

where G_{shell} is the Greens function at the first site of the semi-infinite chain of rings that form the superconducting shell. For details on how this expression is derived and discretized, see Ref. 31, Sec. III-A. The inclusion of this term and a thick semiconductor does not affect the decomposition in m_J modes neither the rotation to eliminate angular dependence, so the effective Hamiltonian of the system reads

$$\tilde{H}_{BdG} = \left[\frac{\left(m_J - \frac{1}{2}\sigma_z - \frac{1}{2}n\tau_z + eA_\varphi(r)r\tau_z\right)^2}{2m^*r^2} + \frac{k_z^2 + p_r^2}{2m^*} \right.$$
$$+ U_0 - \frac{\alpha}{r}\left(m_J - \frac{1}{2}\sigma_z - \frac{1}{2}n\tau_z + eA_\varphi(r)r\tau_z\right)\sigma_z$$
$$+ \alpha k_z \sigma_y \left] \tau_z \right.$$
$$+ \Sigma_{shell}(0).$$
$$(18)$$

Notice that we have substituted $\mu \to -U_0$ to set the conduction band electrostatic potential. For this section, we will take it as radially constant.

B. LDOS: from hollow to solid-core

We now perform several TB calculations for this Hamiltonian as we did in the previous section. We allow the radial coordinate to expand between R_{axis} and $R_{core} = R_{shell} = 70$nm, giving thus a finite thickness to the semiconductor. The 8 simulations of the LDOS as a function of the magnetic flux performed are shown in Fig. 7. As we can no longer use the phase diagram obtained before, we have settled some criteria to choose the parameters: (1) only 7 m_J modes allowed in the first lobe for $\alpha = 0$, (2) Topological region visible in the first lobe for all radii studied and (3) 10 radial sites for all simulations. These conditions could lead to other configurations than those used, but the qualitative features do not change. Since this tubular systems with constant potential are not experimentally doable as presented in this section, we have not considered if the concrete values chosen for U_0 and α are realistic or not.

For $R_{axis} = 69$nm, panel (b), we find a very similar situation to the hollow-core. The only significant difference is the clear definition of the gap edge in the shape of a dome due to the better implementation of the proximity effect we use in this model. CdGM analog states are repealed from it, specially at the center of each lobe, causing the degeneracy point to shift to a lower energy.
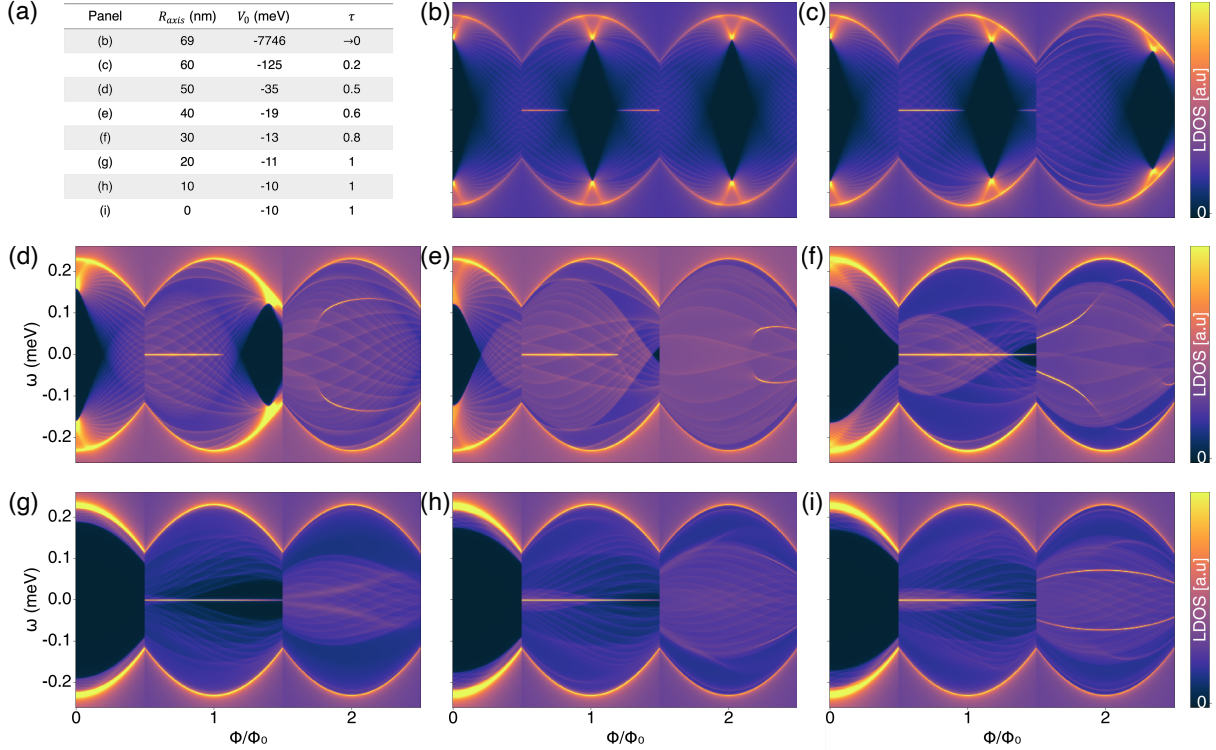
Figure 7. LDOS at the end of semi-infinite tubular nanowires with different thickness in the topological regime.
Using $\Delta_0 = 0.23$meV, $m^* = 0.023$, $m_s = 1$, $\gamma = 2$ and $R_{core} = R_{shell} = 70$nm, we have chosen the parameters shown in panel **(a)** so that there are 7 m_J subbands in the first lobe contributing to the LDOS with $\alpha = 0$. We set $\alpha = 370$meVnm so there is a topological region in all simulations. Discretization parameters $a_s = 0.01$nm and a_0 are chosen so that there are always 10 radial sites. In these simulations we model the superconducting proximity effect with a frequency-dependent self energy (in contrast to the zero-energy approximation used in Fig. 5). In this way, the parent superconductor gap edge is more defined and all CdGM analog features remain below the parent gap. **(b)** For $R_{axis} \approx R_{core}$ we obtain essentially the same behaviour as in the previous section (see Fig. 5), but the degeneracy point has shifted to a lower energy due to the frequency-dependent self energy. Moreover, the introduction of a strong SOC increases the effective doping of the nanowire and many more m_J modes to contribute to the LDOS. **(c-e)** As we increase the thickness of the semiconductor tube, $R_{core} - R_{axis}$, the degeneracy point shifts to larger magnetic fluxes within each lobe (faster the larger n), even disappearing below the next lobe. The CdGM-Van Hove states get correspondingly skewed towards larger fluxes. The system gap (in black) that is mostly localized below the degeneracy point also shifts to the right. The topological phase transitions in the first lobe are also displaced to larger fluxes, up to the point that the right ZBP disappears while the left one extends more throughout the first lobe. Note that in (e) the gap in the first lobe disappears. **(f-i)** The topological phase transitions are no longer visible and the left ZBP extends throughout the whole first lobe. In the solid-core limit, (i), there is no topological gap whatsoever separating the Majorana zero mode from the continuum of subgap LDOS coming from $m_J \neq 0$ CdGM analog states.

The SOC parameter has allowed many more m_J modes to contribute, reducing the true gap of the system to a thin rhomb in the center of the lobe. The borders of this figure are in the $m_J = 0$ mode, and we deduce that they are associated to $k_z = 0$ since they mark topological transitions. The degeneracy point is slightly shifted from the center of the lobe, causing the Majorana ZBPs to be slightly asymmetric. This shift is greater in the second lobe, but non-existent in the zeroth one.

As we increase the thickness of the semiconductor in panel (c), with $R_{axis} = 60$nm, the shift of the degeneracy point is much more noticeable and the lobes stop to be periodically repeated. Eventually, for $R_{axis} = 40$nm, panel (d to e), the degeneracy point is outside the first

lobe, in a metastable region with fixed fluxoid for all fluxes. In the hollow-core model, we showed that the degeneracy point appears for integer fluxes. However, the wave functions are now allowed to exist in a region between R_{axis} and R_{core}, the effective magnetic flux they experience is lowered with respect to that of the superconducting shell. This causes the degeneracy point to shift towards higher magnetic fields. Approximately, the flux at which we find the degeneracy point Φ_{dp} is for the first lobe [31].

$$\frac{\Phi_{dp}}{\Phi_0} = \frac{R_{LP}^2}{R_{av}^2}, \qquad (19)$$

where $R_{LP} = (R_{core} + R_{shell})/2$ and $R_{av} = (R_{axis} +$

$R_{core})/2$.

In panels (b) to (i), we have seen that the *left* ZBP associated to a MBS increases its length following the shift of the degeneracy point. This is easily understandable, as the CdGM-Van Hove state to which the topological transition is associated is affected by the change of effective flux like every other in-gap state. It is remarkable that for panels (h) to (i) we are not able to observe the topological transition. This situation is pretty similar to the one shown in Fig. 6, with the exception that now all topological transitions are metastable. By manual exploration of the parameter set, we have observed that for the solid-core with constant electrostatic potential the topological region is huge in the metastable fixed fluxoid regime, so, to see the topological transition inside the stable region requires fine-tuning.

While for some values of R_{axis} the ZBP of the MBS is located over a true gap, at least for some fluxes (see panel (g)), for others it is fully located over a quasi-continuum of CdGM analogs. Of course, the topological gap is still a true gap for the $m_J = 0$ mode in all cases.

Focusing now on the second lobe, the shift of the degeneracy point as we lower R_{axis} is more pronounced, loosing even the true gap of the system for $R_{axis} = 50$nm (panel (d)). In some cases (panels e,f and i), we also notice that, while most CdGM-Van Hove states behave similarly to those in the first and zeroth lobe (but covering the whole lobe), a pair of those states associated to $m_J = \pm 1/2$ is different, their curvature does not resemble the others We are not even able to see their crossing at 0 energy as that region is barely populated on their respective mode LDOS. This special behavior of $m_J = \pm 1/2$ is not present for all other radii.

Finally, the zeroth lobe does not show anything interesting for none of the cases. Its CdGM analog states get closer to the dome as we augment the transparency of the junction (behavior that of course repeats in all other lobes). Apart from that, it is not affected by the increase of thickness.

V. SOLID-CORE NANOWIRE

A. Model

To obtain what we call a solid-core nanowire, it is *a priori* enough to set $R_{axis} = 0$ in the system we used in the previous section. However, a good model has to take in account the mismatch between the work functions of the semiconductor and the superconductor. This produces an ohmic-type semiconductor band bending at the interface, so the electrostatic potential of the semiconductors conduction band cannot be considered constant, but dome-like [40]. In consequence, a quantum well is created at the interface where we find a charge accumulation, as schematically depicted in Fig. 8. The system, specially its LDOS, resembles more one of the tubular models with finite R_{axis} studied in the previous section
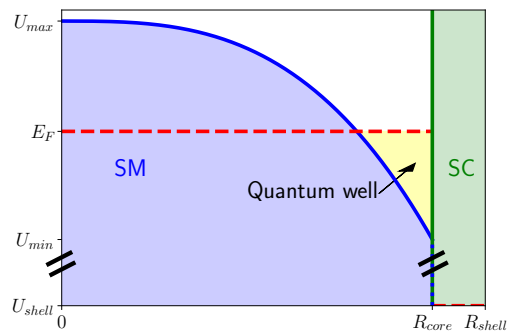

Figure 8. **Sketch of the electrostatic potential profile used for the realistic solid-core nanowire model.** The work function difference between the semiconductor and the superconductor produces a semiconductor conduction-band bending close to InAs/Al interface. It has a dome-like radial profile with maximum value at the center, U_{max}, and minimum value at the super- conductor/semiconductor interface, U_{min}, that typically lies below the Fermi level, see blue curve. The conduction band bottom of the superconductor has a much larger negative energy, $|U_{shell}| \gg |U_{max}|$. Due to the velocity mismatch between both materials, a quantum well forms close to the interface where the charge accumulates, creating as a result an effective tubular nanowire as those explored in Sec. IV.

than the proper solid-core with constant potential and $R_{axis} = 0$. The width of this quantum well determines to which of those models the system is "equivalent", the greater width, the greater the thickness. We take that the potential dome profile is [31]

$$U(r) = U_{min} + (U_{max} - U_{min}) \left(\frac{r}{R_{core}} \right)^3, \quad (20)$$

as for Al/InAs, $U_{shell} \gg U_{max}$. This also has an effect on the SOC, as it is now radial dependent. In a typical 8-band model [41, 42]

$$\alpha \rightarrow \alpha(r) = \alpha_0 \frac{dU(r)}{dr}, \quad (21)$$

with the prefactor

$$\alpha_0 = \frac{P^2}{3} \left[\frac{1}{\Delta_g^2} - \frac{1}{(\Delta_s + \Delta_g)^2} \right], \quad (22)$$

where, for InAs, we use the Kane parameter $P = 919.7$meVnm, the semiconductor gap $\Delta_g = 417$meV and the split-off gap $\Delta_s = 390$meV, obtaining $\alpha_0 = 1.19$nm^2. Again, this does not affect any of the symmetry considerations we used to simplify the effective Hamiltonian, so

we have

$$\tilde{H}_{BdG} = \left[\frac{\left(m_J - \frac{1}{2}\sigma_z - \frac{1}{2}n\tau_z + eA_\varphi(r)r\tau_z\right)^2}{2m^*r^2} + \frac{k_z^2 + p_R^2}{2m^*} \right.$$
$$+ U(r) - \frac{\alpha(r)}{r}\left(m_J - \frac{1}{2}\sigma_z - \frac{1}{2}n\tau_z + eA_\varphi(r)r\tau_z\right)\sigma_z$$
$$+ \left. \alpha(r)k_z\sigma_y\right]\tau_z$$
$$+ \Sigma_{shell}(0),$$
(23)

where the only change with respect to (18) is the introduction of the radial dependence in the potential, $U_0 \to U(r)$ and the Rashba term $\alpha \to \alpha(r)$.

B. Local density of states

As we have done in the previous sections, we simulate the LDOS at the end of the wire for three different configurations shown in Fig. 9. For the nominal value of α_0 obtained through (22) we need to carefully fine-tune the potential profile in order to find ZBPs. Thus, for the sake of clarity, we have opted to use an order of magnitude higher value of α_0 to illustrate the topological regime. Comparing it with the non-topological one, panels (b) vs (a), we observe that the only qualitative difference is the emergence of the Majorana ZBPs. Specifically, only the $m_J = 0$ of odd LP lobes is significantly affected by the apparition of topology, as pictured in panels (d) and (e). All other CdGM analogs, both with integer and half-integer m_J, barely undergo quantitative changes. This outcome was already predicted in the oversimplified model of Sec. III. For completeness, in this section we have simulated up to the third LP lobe to point out that topology is also present in all odd lobes.

The introduction of a dome-profile potential spatially creates a higher density of charge in a ring region more or less close to the interface and thin depending on its exact shape. Thus, a solid-core with such potential should in some way resemble a tubular model with a given inner radius, as long as all other parameters remain the same or equivalent. However, in our tubular Hamiltonian we used a constant Rashba term, not radially dependent. In consequence, we cannot establish a direct relation between the models. Yet, as we have just explained, the effect of SOC is mainly introduced in the $m_J = 0$ mode and, what is more, barely affects the position of the degeneracy point. Hence, a visual comparison between Figs. 9(a) and 7(d-e) allows as to say that our solid-core dome profile model resembles a tubular model with $R_{axis} \sim 40 - 50$nm. There exists nevertheless a significant difference in the topological regime (Fig. 9(b)), as in a tubular model with such a thickness it has been impossible to find a Majorana ZBP that extends throughout the full lobe. On the other hand, we have had the opposite problem in the solid-core dome-profile model, where to find a topological transition visible inside the first lobe we require fine-tuning of the potential.

Additionally, in Fig. 9(c,f), we have added a finite thickness to the superconducting shell and a Zeeman potential to the Hamiltonian,

$$V_z = \frac{1}{2}g\mu_B B\sigma_z = \frac{1}{2}g\mu_B \frac{\Phi}{\pi R_{LP}^2}\sigma_z,$$
(24)

with μ_B the Bohr magneton and g the Landé g factor. These up to now ignored effects only further shift the degeneracy point in flux, but otherwise have a small effect on the wire's spectrum.

VI. CONCLUSIONS

In this master thesis, we have studied the effect of the SOC in full-shell Majorana nanowires from analytical calculations and from numerical simulations of the bandstructure and the LDOS. We have used a cylindrical approximation for the hybrid nanowire and three different models of increasing complexity. Starting from the simplest hollow-core nanowire approximation, we have decomposed the Hamiltonian in generalized angular momentum subbands, where m_J is a good quantum number, to get rid of the angular dependence. In the first approach, that can be solved analytically, the semiconductor is assumed to have negligible thickness and be concentrated at the superconductor/semiconductor interface. Then, we allow for the semiconductor to acquire a certain thickness, in what we have called the tubular model. Finally, we study a solid-core nanowire where we take in account the mismatch of Fermi energies between the metallic shell and the semiconductor core through a dome-profile electrostatic potential. The superconducting proximity effect of the shell on the core is taken into account approximately by integrating-out the superconductor and introducing its effect as a self-energy term at the boundary of the semiconductor. We now discuss the general results and conclusions of the three approaches.

Firstly, in Sec. III, we have analytically observed the most important effects of the SOC in the hollow-core nanowire. Studying the bandstructure (for simplicity without LP gap modulation), we have shown how α breaks the subband degeneracy, but barely shifts in energy most of the subbands, specially their minimum points. These points are of special interest, since they generate Van Hove singularity peaks in the LDOS at the end of a semi-infinite wire that we call CdGM analog states. We have also approximated these states in the LDOS by analytically calculating all band minima as a function of the flux. By doing so, we conclude that the most dispersing angular momentum mode with flux is $m_J = 0$, as finite m_J modes are essentially dispersionless for high enough α. This was expected, as the topological phase transition of the system necessarily occurs by a zero energy crossing with flux of the CdGM analog state associated to $m_J = 0$ and $k_z = 0$, as we have also explored. From these calculations, we have obtained a topological phase diagram of the system and the range
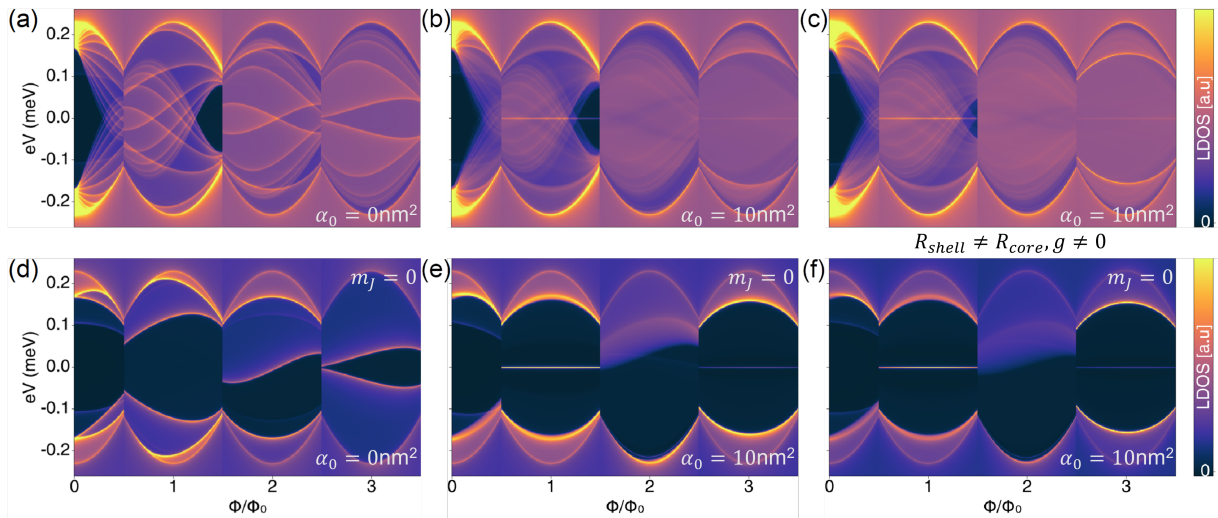
Figure 9. **LDOS as a function of the magnetic flux at the end of a semi-infinite solid-core nanowire with a realistic radial dome-profile electrostatic potential.** Upper row: total LDOSdisplaying half of the $n = 0$ lobe, and $n = 1, 2, 3$ LP lobes. Lower row: LDOS of the lowest-energy subband, which corresponds to $m_J = 0$ in odd lobes and $m_J = 1/2$ in even ones. The potential is as in Eq. (20) with $U_{min} = -70$meV and $U_{max} = 0$meV. **(a,b)** The only qualitative difference between the case without (a) and with (b) SOC is the emergence of a ZBP through the first and third lobes. The behavior of the CdGM-Van Hove states does not change significantly. **(d,e)** Focusing only on the $m_J = 0$ mode, the inclusion of SOC changes dramatically the LDOS due to the appearance of the ZBP. **(c,f)** Introducing a realistic R_{shell} (to simulate a superconducting shell thickness) and a Zeeman parameter g shifts the degeneracy point to larger flux values. This reduces the shifted gap and skews the CdGM analog states, including the Majorana zero mode. Comparing (b) with Fig. 7 we observe that the LDOS is pretty similar to that of a tubular model with $R_{axis} \sim 40 - 50$nm. Parameters not mentioned are as in Fig. 7.

in flux of the topological region for any set of parameters. Including the LP effect, we observe that it allows to obtain topology for smaller values of the SOC parameter and the chemical potential. The Majorana ZBP in the hollow-core approximation is typically present only at the edges of the odd LP lobes. To have it expand all across the odd lobe, very high values of α and μ are required. Then, we have computed the LDOS as a function of the magnetic flux at the edge of the nanwoire, in a non-destructive LP regime, discretizing the system into a TB Hamiltonian for several values of α, to confirm our analytical predictions. We have observed symmetrical ZBPs at the edges of the first lobe according to the phase diagram, with topological transitions at the zero-energy crossings of the $m_J = 0, k_z = 0$ subgap state, and first order magnetic transitions at the lobe edges. We have observed a degeneracy point of all the CdGM analogs at the center of each lobe and with energy Δ_0. We have also simulated the LDOS for a wide range of the magnetic flux but artificially fixing the fluxoid to $n = 1$. In this way, we have been able to examine metastable regions of the flux where we have found the other pair of analytically predicted topological phase transitions associated to the Majorana ZBPs that appear at the edges of the first lobe.

Secondly, in Sec. IV, we have consider a more realistic scenario where the semiconductor has a finite thickness. We have also checked the effects of using a self-energy

to introduce the proximity effect. The superconducting gap edge gets clearly defined in the LDOS and all subgap states remain at energies below the parent gap. The wire's finite thickness results in a displacement of the degeneracy point within each lobe to larger values of $|\Phi|$. For the extremely thin hollow-core, it is situated exactly at integer normalized fluxes, but for tubular ones the degeneracy point shifts with the thickness. The shift is proportional to the fluxoid number of the difrent lobes, being the zeroth lobe unaffected, and in consequence breaking the symmetry around the center of each lobe. The degeneracy points can even be displaced to metastable regions of the flux, i.e., away form the LP lobes, effectively loosing them from the LDOS, but their effects are still observable over the subgap states, as they acquire a skeweness towards larger values of flux. The effective wire's gap (that is maximum below the degeneracy points), also gets shifted to the LP lobe edges, disappearing for good for sufficient tube thickness. We have observed that the SOC qualitatively affects the system in the same way as with the previous model, but in this case the ZBPs extends to larger flux values as the degeneracy point shifts with semiconductor thickness. In the solid-core limit, with a radially constant electrostatic potential (constant μ), the ZBPs associated to the end MBS expand throughout the whole odd lobes. In order to be able to see topology for all radii studied, we have used a very large SOC parameter, but for larger thicknesses,

smaller values of α are needed to observe Majorana zero modes. The Majorana ZBP has a minigap for the $m_J = 0$ LDOS, however, the complete LDOS does not typically present a topological minigap between the zero energy mode and the continuum of states produced by the other m_J modes.

Thirdly, in Sec. V we have explored a more realistic model of a solid-core nanowire in which we have set a radial dome-profile electrostatic potential for the conduction band bottom of the semiconductor that induces charge accumulation close to the core/shell interface, leading to results that can be compared to a tubular model with a certain semiconductor thickness. We have illustrated that the main effect of the topological regime is the appearance of a Majorana ZBP in the $m_J = 0$ mode, while all other CdGM-Van Hove states remain qualitatively the same, specially the position in magnetic flux of the degeneracy point. The degeneracy point flux in turn allows to indentify an equivalent tubular model for the description of the hybrid nanowire. However, the behavior of the ZBPs is not the same as in the tubular model, as it expands throughout all the odd LP lobe. In the corresponding tubular model, a topological transition is always visible inside the lobe. We have also added a finite thickness to the superconductor and switched on the Zeeman effect in order to demonstrate that their only effect is further shifting the degeneracy point in flux, with no other relevant qualitative consequence.

In conclusion, we have demonstrated that the SOC does not significantly change the behavior of the CdGM analog states, except for those associated to the $m_J = 0$ subband. This is specially true for the Van Hove singularity at $k_z = 0$, that changes dramatically with SOC and drives the topological phase transition of the system. For a realistic full-shell nanowire with a dome-profile electrostatic potential, the degeneracy point shifts with respect to the lobe center (for all $n \neq 0$ LP lobes) and it even disappears from the visible LP flux extension. This creates a shifted, small gap if present, and it skews the CdGM-Van Hove singularities towards larger fluxes within each lobe, the more the larger the fluxoid number n. In the topological phase, the MBS ZBPs that appear at the odd lobe edges in the hollow-core approximation, extends over wider flux ranges. In particular, for positive fluxes, the right ZBP disappears form the odd lobes, while the left one extends towards the other side of the lobe as the semiconductor charge-density distribution acquires a finite thickness. In general, for what we consider are realistic parameters of the dome profile, the ZBP extends throughout all the odd LP lobes. It should be noted nevertheless that the precise shape of this electrostatic potential is unknown and cannot be access directly with an experiment. Actually, the comparison of experimental results of tunneling spectroscopy with our LDOS simulations could be used to access microscopic parameters of these wires in an indirect way. Let us also notice that in realistic solid-core nanowires and considering the cylindrical approximation we have used for this wires, there is typically no topological minigap separating the Majorana zero mode from the continuum of states present inside the LP gap due to $m_J \neq 0$ CdGM analog states. This is detrimental for the use of these states as topological qubits. Nevertheless, it has been suggested that a small quantity of symmetry breaking or disorder could open small topological minigaps [15, 19].

For the future, there is still more work to do in order to better describe the realistic experimental scenario, such as considering the hexagonal shape of the nanowire cross-section, including the superconductor at the TB level, including disorder, both in the transverse and longitudinal directions, considering finite nanowire length effects and, finally, computing the differential conductance dI/dV to truly compare to experiments.

METHODS

All our tight-binding simulations have been computed using Quantica.jl [43].

[1] E. Prada, P. San-José, M. W. de Moor, A. Geresdi, E. J. Lee, J. Klinovaja, D. Loss, J. Nygard, R. Aguado, and L. P. Kouwenhoven, From andreev to majorana bound states in hybrid superconductor-semiconductor nanowires, Nature Review Physics **2**, 575 (2020).

[2] C. Beenakker, Search for majorana fermions in superconductors, Annual Review of Condensed Matter Physics **4**, 113 (2013).

[3] R. Aguado, Majorana quasiparticles in condensed matter, La Rivista del Nuovo Cimento **40**, 523 (2017).

[4] T. D. Stanescu and S. Tewari, Majorana fermions in semiconductor nanowires: fundamentals, modeling, and experiment, Journal of Physics: Condensed Matter **25**, 233201 (2013).

[5] M. Sato and Y. Ando, Topological superconductors: a review, Reports on Progress in Physics **80**, 076501 (2017).

[6] M. Leijnse and K. Flensberg, Introduction to topological superconductivity and majorana fermions, Semiconductor Science and Technology **27**, 124003 (2012).

[7] A. Y. Kitaev, Unpaired majorana fermions in quantum wires, Physics-Uspekhi **44**, 131 (2001).

[8] L. Fu and C. L. Kane, Superconducting proximity effect and majorana fermions at the surface of a topological insulator, Phys. Rev. Lett. **100**, 096407 (2008).

[9] R. M. Lutchyn, J. D. Sau, and S. Das Sarma, Majorana fermions and a topological phase transition in semiconductor-superconductor heterostructures, Phys. Rev. Lett. **105**, 077001 (2010).

[10] Y. Oreg, G. Refael, and F. von Oppen, Helical liquids and majorana bound states in quantum wires, Phys. Rev. Lett. **105**, 177002 (2010).

[11] V. Mourik, K. Zuo, S. M. Frolov, S. R. Plissard, E. P. A. M. Bakkers, and L. P. Kouwenhoven, Signatures of majorana fermions in hybrid superconductor-semiconductor nanowire devices, Science **336**, 1003 (2012).

[12] F. Nichele, A. C. C. Drachmann, A. M. Whiticar, E. C. T. O'Farrell, H. J. Suominen, A. Fornieri, T. Wang, G. C. Gardner, C. Thomas, A. T. Hatke, P. Krogstrup, M. J. Manfra, K. Flensberg, and C. M. Marcus, Scaling of majorana zero-bias conductance peaks, Phys. Rev. Lett. **119**, 136803 (2017).

[13] M. T. Deng, S. Vaitiekenas, E. B. Hansen, J. Danon, M. Leijnse, K. Flensberg, J. Nygård, P. Krogstrup, and C. M. Marcus, Majorana bound state in a coupled quantum-dot hybrid-nanowire system, Science **354**, 1557 (2016).

[14] A. C. Potter and P. A. Lee, Engineering a $p+ip$ superconductor: Comparison of topological insulator and rashba spin-orbit-coupled materials, Phys. Rev. B **83**, 184520 (2011).

[15] S. Vaitiekenas, G. W. Winkler, B. van Heck, T. Karzig, M.-T. Deng, K. Flensberg, L. I. Glazman, C. Nayak, P. Krogstrup, R. M. Lutchyn, and C. M. Marcus, Flux-induced topological superconductivity in full-shell nanowires, Science **367**, 10.1126/science.aav3392 (2020).

[16] S. Vaitiekenas, P. Krogstrup, and C. M. Marcus, Anomalous metallic phase in tunable destructive superconductors, Phys. Rev. B **101**, 060507(R) (2020).

[17] D. Sabonis, O. Erlandsson, A. Kringhøj, B. van Heck, T. W. Larsen, I. Petkovic, P. Krogstrup, K. D. Petersson, and C. M. Marcus, Destructive little-parks effect in a full-shell nanowire-based transmon, Phys. Rev. Lett. **125**, 156804 (2020).

[18] A. Vekris, J. C. Estrada Saldaña, J. de Bruijckere, S. Lorić, T. Kanne, M. Marnauza, D. Olsteins, J. Nygård, and K. Grove-Rasmussen, Asymmetric little–parks oscillations in full shell double nanowires, Scientific Reports **11**, 19034 (2021).

[19] F. Peñaranda, R. Aguado, P. San-Jose, and E. Prada, Even-odd effect and majorana states in full-shell nanowires, Phys. Rev. Research **2**, 023171 (2020).

[20] M. Valentini, F. Peñaranda, A. Hofmann, M. Brauns, R. Hauschild, P. Krogstrup, P. San-Jose, E. Prada, R. Aguado, and G. Katsaros, Nontopological zero-bias peaks in full-shell nanowires induced by flux-tunable Andreev states, Science **373**, 82 (2021).

[21] W. A. Little and R. D. Parks, Observation of quantum periodicity in the transition temperature of a superconducting cylinder, Phys. Rev. Lett. **9**, 9 (1962).

[22] R. D. Parks and W. A. Little, Fluxoid quantization in a multiply-connected superconductor, Phys. Rev. **133**, A97 (1964).

[23] Y. Liu, Y. Zadorozhny, M. M. Rosario, B. Y. Rock, P. T. Carrigan, and H. Wang, Destruction of the global phase coherence in ultrathin, doubly connected superconducting cylinders, Science **294**, 2332 (2001), https://science.sciencemag.org/content/294/5550/2332.full.pdf.

[24] M. Tinkham, Introduction to Superconductivity, 2nd ed. (McGraw-Hill, New York, 1996).

[25] P. de Gennes, Superconductivity of Metals and Alloys (W.A. Benjamin, 1999).

[26] G. Schwiete and Y. Oreg, Persistent current in small superconducting rings, Phys. Rev. Lett. **103**, 037001 (2009).

[27] G. Schwiete and Y. Oreg, Fluctuation persistent current in small superconducting rings, Phys. Rev. B **82**, 214514 (2010).

[28] C. Caroli, P. D. Gennes, and J. Matricon, Bound fermion states on a vortex line in a type ii superconductor, Phys. Lett. **9**, 307 (1964).

[29] E. Brun Hansen, The bound excitations of a single vortex in a pure type ii superconductor, Physics Letters A **27**, 576 (1968).

[30] J. Bardeen, R. Kümmel, A. E. Jacobs, and L. Tewordt, Structure of vortex lines in pure superconductors, Phys. Rev. **187**, 556 (1969).

[31] P. San-Jose, C. Payá, C. M. Marcus, S. Vaitiekėnas, and E. Prada, Theory of caroli-de gennes-matricon analogs in full-shell nanowires (2022).

[32] R. M. Lutchyn, T. D. Stanescu, and S. Das Sarma, Search for majorana fermions in multiband semiconducting nanowires, Phys. Rev. Lett. **106**, 127001 (2011).

[33] M. Valentini, M. Borovkov, E. Prada, S. Marti-Sanchez, M. Botifoll, A. Hofmann, J. Arbiol, R. Aguado, P. San-Jose, and G. Katsaros, Majorana-like coulomb spectroscopy in the absence of zero bias peaks (2022).

[34] F. London, Superfluids, Vol. 1 (Wiley, New York, 1950).

[35] W. Meissner and R. Ochsenfeld, Ein neuer effekt bei eintritt der supraleitfähigkeit, Naturwissenschaften **21**, 787 (1933).

[36] H. Essén and M. C. N. Fiolhais, Meissner effect, diamagnetism, and classical physics—a review, Am. J. Phys. **80**, 164 (2012), https://doi.org/10.1119/1.3662027.

[37] S. Sanvito, C. J. Lambert, J. H. Jefferson, and A. M. Bratkovsky, General green's-function formalism for transport calculations with spd hamiltonians and giant magnetoresistance in co- and ni-based magnetic multilayers, Phys. Rev. B **59**, 11936 (1999).

[38] J. C. Cuevas, A. Martín-Rodero, and A. L. Yeyati, Hamiltonian approach to the transport properties of superconducting quantum point contacts, Phys. Rev. B **54**, 7366 (1996).

[39] T. D. Stanescu and S. Das Sarma, Proximity-induced low-energy renormalization in hybrid semiconductor-superconductor majorana structures, Phys. Rev. B **96**, 014510 (2017).

[40] A. E. G. Mikkelsen, P. Kotetes, P. Krogstrup, and K. Flensberg, Hybridization at superconductor-semiconductor interfaces, Phys. Rev. X **8**, 031040 (2018).

[41] R. Winkler, S. Papadakis, E. De Poortere, and M. Shayegan, Spin-orbit coupling effects in two-dimensional electron and hole systems, Vol. 191 (Springer, 2003).

[42] S. D. Escribano, A. L. Yeyati, and E. Prada, Improved effective equation for the rashba spin-orbit coupling in semiconductor nanowires, Phys. Rev. Research **2**, 033264 (2020).

[43] P. San-Jose, Quantica.jl: a quantum lattice simulation library in the Julia language (2021).